Published in final edited form as:
Nat Struct Mol Biol. 2013 July ; 20(7): 804–813. doi:10.1038/nsmb.2600.

Structural basis for diverse N-glycan recognition by HIV-1–neutralizing V1–V2–directed antibody PG16

Marie Pancera[1,11], **Syed Shahzad-ul-Hussan**[2,11], **Nicole A Doria-Rose**[1,11], **Jason S McLellan**[1], **Robert T Bailer**[1], **Kaifan Dai**[1], **Sandra Loesgen**[2], **Mark K Louder**[1], **Ryan P Staupe**[1], **Yongping Yang**[1], **Baoshan Zhang**[1], **Robert Parks**[3], **Joshua Eudailey**[3], **Krissey E Lloyd**[3], **Julie Blinn**[3], **S Munir Alam**[3], **Barton F Haynes**[3], **Mohammed N Amin**[4,5], **Lai-Xi Wang**[4,5], **Dennis R Burton**[6,7,8,9], **Wayne C Koff**[10], **Gary J Nabel**[1], **John R Mascola**[1], **Carole A Bewley**[2], and **Peter D Kwong**[1]

[1]Vaccine Research Center, National Institute of Allergy and Infectious Diseases, US National Institutes of Health, Bethesda, Maryland, USA

[2]Laboratory of Bioorganic Chemistry, National Institute of Diabetes and Digestive and Kidney Diseases, US National Institutes of Health, Bethesda, Maryland, USA

[3]Duke Human Vaccine Institute, Duke University Medical Center, Durham, North Carolina, USA

[4]Institute of Human Virology, University of Maryland School of Medicine, Baltimore, Maryland, USA

[5]Department of Biochemistry and Molecular Biology, University of Maryland School of Medicine, Baltimore, Maryland, USA

[6]Department of Immunology and Microbial Science, Scripps Research Institute, La Jolla, California, USA

[7]International AIDS Vaccine Initiative Neutralizing Antibody Center, Scripps Research Institute, La Jolla, California, USA

[8]Ragon Institute of Massachusetts General Hospital, Massachusetts Institute of Technology and Harvard University, Cambridge, Massachusetts, USA

[9]Center for HIV/AIDS Vaccine Immunology and Immunogen Discovery, The Scripps Research Institute, La Jolla, California, USA

Correspondence should be addressed to C.A.B. (caroleb@mail.nih.gov) or P.D.K. (pdkwong@nih.gov).
[11]These authors contributed equally to this work

Accession code: Structure factors and coordinates for the cocrystal structure of PG16 with glycosylated V1–V2 have been deposited with the Protein Data Bank under accession code 4DQO.

Note: Supplementary information is available in the online version of the paper.

Author Contributions: M.P., S.S.-u.-H., N.A.D.-R., J.S.M., B.F.H., G.J.N., J.R.M., C.A.B. and P.D.K. designed research and analyzed the data; M.P., S.S.-u.-H., N.A.D.-R., R.T.B., K.D., M.K.L., S.L., R.P.S., Y.Y., B.Z., R.P., J.E., K.E.L., J.B. and S.M.A. performed research; D.R.B. and W.C.K. contributed PG9 and PG16 antibodies; M.N.A. and L.-X.W. contributed N-glycans; M.P., S.S.-u.-H., N.A.D.-R., C.A.B. and P.D.K. wrote the paper, with all principal investigators providing comments or revisions.

Competing Financial Interests: The authors declare no competing financial interests.

[10]International AIDS Vaccine Initiative, New York, New York, USA

Abstract

HIV-1 uses a diverse N-linked-glycan shield to evade recognition by antibody. Select human antibodies, such as the clonally related PG9 and PG16, recognize glycopeptide epitopes in the HIV-1 V1–V2 region and penetrate this shield, but their ability to accommodate diverse glycans is unclear. Here we report the structure of antibody PG16 bound to a scaffolded V1–V2, showing an epitope comprising both high mannose–type and complex-type N-linked glycans. We combined structure, NMR and mutagenesis analyses to characterize glycan recognition by PG9 and PG16. Three PG16-specific residues, arginine, serine and histidine (RSH), were critical for binding sialic acid on complex-type glycans, and introduction of these residues into PG9 produced a chimeric antibody with enhanced HIV-1 neutralization. Although HIV-1–glycan diversity facilitates evasion, antibody somatic diversity can overcome this and can provide clues to guide the design of modified antibodies with enhanced neutralization.

The HIV-1 envelope spike (Env) is the primary target of HIV-1–neutralizing antibodies and is heavily glycosylated, especially in its gp120 component, with N-linked glycans contributing approximately half the spike mass and covering most of the spike surface (reviewed in refs. 1,2). Despite the prominent coverage of Env surface by N-linked glycan, sera and antibodies from HIV-1–infected individuals generally show minimal glycan-dependent reactivity[3–5]. The low frequency of glycan-reactive antibodies has been attributed to issues of cross-reactivity in antibody recognition of N-linked glycan on HIV-1 Env and of N-linked glycan on host or self proteins. Indeed, the antigenic structure of HIV-1 gp120 displays a ‘silent face’ that corresponds to a dense cluster of N-linked glycans[6,7], which is infrequently recognized by the host immune system.

The 2G12 antibody[8], which recognizes a cluster of high mannose–type glycans on HIV-1 gp120 (refs. 9,10), provided an early notable exception to this general lack of N-glycan reactivity[3,11], and in recent years, a number of other N-glycan–reactive HIV-1–neutralizing antibodies have been isolated from the sera of HIV-1–infected donors[12,13]. Characterization of these antibodies is ongoing, but all appear to recognize either an array of N-linked glycans in a multivalent manner (2G12)[9,10,14–17] or a combination of N-linked glycan and envelope polypeptide (PG9, PGT128)[18,19] (Supplementary Table 1). Such multicomponent recognition provides a means to reduce the affinity of antibody for individual N-linked glycans to a tolerable level, thereby overcoming issues related to self-reactivity[17,18,20].

A common theme with many of these glycan-reactive antibodies is a requirement for high mannose–type N-linked glycans. Characterization of monomeric HIV-1 gp120 indicated substantial glycan diversity[21–23], with complex-type N-linked glycans present at one-third to one-half of the N-linked sites on gp120. The high density of glycan on the assembled viral spike, however, appears to inhibit glycan processing, and high mannose–type N-linked glycans predominate[24–29]. The percentage of high mannose–type glycans on functional viral spikes appears to depend on several factors including host cell and viral strain[24,25,30], but a substantial diversity of high-mannose types as well as complex types may be present[24,31].

Further, this diversity may have a role in viral infectivity[32,33], cell-mediated viral transmission[34], regulation of spike conformation[31] and immune evasion[7,35,36].

Does glycan variation, such as that between high mannose–type and complex-type glycans, allow for HIV-1 escape from the newly identified glycan-reactive antibodies? Or do these antibodies have mechanisms to cope with glycan diversity? Recent analysis of PGT121 indicated an ability to recognize complex-type N-linked glycans[37], but the absence of a PGT121–gp120 structure has made it difficult to understand the context of this recognition. To address these questions, we extended our characterization of broadly neutralizing antibodies that target the V1–V2 region of gp120 and require a high mannose-type N-linked glycan at residue 160_{gp120} for HIV-1 neutralization[13]. (For clarity, we add the macromolecule as a subscript when referring to specific residues.) This category of broadly neutralizing antibodies includes three sets of somatically related antibodies: PG9 and PG16 from donor IAVI 24, PGT141–145 from donor IAVI 84 and CH01–CH04 from donor CHAVI 0219. These individually neutralize 70–80%[13], 40–80%[38] and 40–50%[5], respectively, of circulating HIV-1 isolates. An even higher level of breadth is achieved when somatic variants are combined: for example, the combined neutralization of PG9 and PG16 reaches ∼90% of circulating HIV-1 isolates[18]. Among these V1–V2–directed antibodies, the structure of PG9 in complex with the V1–V2 domain of gp120 was solved and revealed cooperative recognition by PG9 of strand C of V1–V2 and two N-linked glycans attached at residue 160_{gp120} (N-glycan 160) and either residue 156_{gp120} (in most HIV-1 strains) or residue 173_{gp120} (in specific strains such as ZM109) (N-glycan 156 or 173)[18]. The recognition of N-glycan 160 appeared to be specific to a subset of high mannose–type glycans (such as those with five mannose and two *N*-acetylglucosamine residues ($Man_5GlcNAc_2$))[13], but the recognition of N-glycan 156 or 173 did not appear to be necessarily constrained to high-mannose types.

Here we report the crystal structure of the antigen-binding fragment (Fab) of the PG16 antibody in complex with the V1–V2 domain of HIV-1 gp120 from strain ZM109 along with NMR characterization of glycan recognition by PG16, PG9 and various mutated forms in which we specifically knocked out antibody recognition for either N-glycan 160 or N-glycan 156 or 173. We created a PG9-PG16 chimera with enhanced recognition of complex-type N-linked glycans that retained the clean autoreactivity profile of the parent PG9 and PG16 antibodies. Overall, these analyses describe glycan binding specificities and atomic-level details of the PG16 epitope and reveal how HIV-1 envelope-spike variability can be collectively overcome by somatic mechanisms of clonal antibody diversification.

Results

Structure of PG16 in complex withV1–V2 of HIV-1 gp120

Our interest in diverse glycan recognition by antibody PG16 was spurred by the observation that, when expressed in HEK293F or in HEK293S GnTI$^-$ cells, scaffolded V1–V2s that bound well to PG9 generally showed weak (HEK293F) or no binding (GnTI$^-$) to PG16 (Supplementary Fig. 1a). However, when expressed in HEK293F cells treated before transfection with the α-mannosidase II inhibitor swainsonine (which is predicted to induce hybrid-type glycans with a $Man_5GlcNAc_2$ core), improved binding of scaffolded V1–V2s to

PG16 could be observed (Supplementary Fig. 1a)[39]. To understand how PG16 antibody recognizes HIV-1 gp 120, we determined the structure of PG16 bound to the scaffolded V1–V2 produced in HEK293F cells treated with swainsonine. We obtained the PG16–V1–V2 complex, following procedures that had succeeded with PG16's somatic relative PG9 (ref 18). In particular, immobilization of PG16 IgG onto Protein A–agarose resin allowed us to select appropriately folded scaffolded V1–V2s and then perform on-column protease cleavage of IgG to Fab[18] to obtain homogeneous complexes of PG16 bound to scaffolded V1–V2s (Supplementary Fig. 1b,c). We note that the yield of scaffolded V1–V2 bound to PG16 Fab was low (~2%), and this probably reflects selection of scaffolded V1–V2 containing suitable glycosylation for PG16 recognition. First, we found that lectins that can discriminate between various oligomannosides, and complex-type glycans containing α2–3 or α2–6 sialic acid were able to bind the unselected scaffolded V1–V2s. This indicates that multiple glycoforms are present before PG16 selection (Supplementary Fig. 2a,b and Supplementary Note). Second, MS analyses and glycopeptide mapping of the scaffolded V1–V2 prior to purification with PG16 showed diverse N-linked glycans: 12 glycoforms at $Asn160_{gp120}$ including 20% $Man_5GlcNAc_2$ and 30% hybrid-type glycans; and 13 glycoforms at $Asn173_{gp120}$ including 56% hybrid glycan (Supplementary Fig. 2c–e).

To increase our chances of crystallization, we tested several crystallization variants, including one comprising the 1FD6 scaffolded V1–V2 region from the ZM109 isolate, in which N-glycosylation sites at positions 160 and 173 were preserved, but all of the four other potential N-glycosylation sites on V1–V2 were mutated to alanine. We obtained cocrystals of Fab PG16 in complex with 1FD6 scaffolded ZM109 V1–V2 that diffracted to 2.5-Å resolution (Table 1).

Whereas the structure of PG16 bound to the scaffolded V1–V2 domain of HIV-1 strain ZM109 resembled the previously reported PG9 complex of the same scaffold[18], the presence of a hybrid-type glycan at $Asn173_{gp120}$ of ZM109 V1–V2 was newly observed (Fig. 1). As with PG9, the protruding complementarity-determining region (CDR) H3 of PG16 reached through the glycan shield to contact both glycan and polypeptide, and the V1–V2 domain formed a four-stranded β-sheet displaying a Greek-key motif possessing two disulfide linkages between strands A and B and between A and D (Fig. 1). Superposition of scaffolded V1–V2s complexed to PG9 or PG16 showed a Cα r.m.s. deviation of 1.3 Å, and variable domains' superpositions between PG9 and PG16 resulted in a Cα r.m.s. deviation of 0.6 Å.

PG16–V1–V2 interactions

Several types of interactions arbitrate PG16 recognition of HIV-1 V1–V2. These can be classified into sequence-independent, electrostatic and glycan-mediated interactions (Fig. 2). Sequence-independent interactions are prominent in the PG16–V1–V2 complex, and the protruding CDR H3 of PG16 aligns its most distal β-strand (residues $100E_{HC}$ to $100H_{HC}$ in Kabat nomenclature[40], with HC and LC subscripts for heavy chain and light chain, respectively) in parallel orientation with strand C of V1–V2 to form an intermolecular β-sheet with four hydrogen bonds (Fig. 2b). These sequence-independent interactions are similar to those observed previously in the PG9–V1–V2 complex[18]. Electrostatic

interactions were also observed between PG16 and V1–V2, most prominently a double salt bridge between $Arg168_{gp120}$ and both the side chain of $Asp100L_{HC}$ and the sulfate of the tyrosine-sulfated $100H_{HC}$ ($Tys100H_{HC}$). A salt bridge between $Asp100I_{HC}$ and $Lys171_{gp120}$ was also observed (Fig. 2c). Electrostatic interactions between PG16 and gp120 were less extensive than interactions between PG9 and gp120. In the PG9–V1–V2 complex, two additional electrostatic interactions, between $Tys100G_{HC}$ and $Lys169_{gp120}$ and between $Tyr100K_{HC}$ and $Asn173_{gp120}$, were observed; with PG16, $Tyr100G_{HC}$ is not sulfated, and residue $100K_{HC}$ is an asparagine.

The most prominent interactions occur between PG16 and N- glycans 160 and 173 (Fig. 2d,e). Extensive interactions between PG16 and an N-glycan present at $Asn160_{gp120}$ are observed. From the visualized glycan electron density (Supplementary Fig. 2f), the N-glycan 160 appears to be $Man_5GlcNAc_2$, though it is formally possible that it could be a glycan that shares the $Man_5GlcNAc_2$ substructure but is disordered at residues outside the $Man_5GlcNAc_2$ core. Interactions between this glycan and PG16 bury a total surface area of approximately 1,100 $Å^2$ and form nine intermolecular hydrogen bonds (<3.5 Å; Supplementary Table 2). Eight of these nine hydrogen bonds are formed between the terminal mannose moieties and the side chains of $His100R_{HC}$, $Asn100P_{HC}$, $Asp31_{LC}$, $Ser32_{LC}$ and $Asp50_{LC}$. One hydrogen bond is present between the reducing *N*-acetyl glucosamine of $Man_5GlcNAc_2$ and the side chain of $His100B_{HC}$ in the PG16 CDR H3 (Fig. 2d). Comparison of the interactions of PG16 and PG9 with high-mannose glycans at position 160 showed that the major differences lie in two residues at positions 100_{HC} and $100B_{HC}$ in the CDR H3 (Supplementary Table 2). In PG9, $Asp100_{HC}$ and $Arg100B_{HC}$ contribute one and three hydrogen bonds, respectively, with the protein-proximal *N*-acetyl glucosamine unit of $Man_5GlcNAc_2$ 160_{gp120}, whereas $Ile100_{HC}$ and $His100B_{HC}$ in PG16 contribute zero and one hydrogen bond, respectively (Fig. 2d and Supplementary Table 2).

PG16 also interacts extensively with an N-linked hybrid-type glycan present at $Asn173_{gp120}$, burying a total surface area of 800 $Å^2$ at the antibody-glycan interface and contributing six hydrogen bonds (<3.5 Å; Supplementary Table 2). In particular, interactions between PG16 and the terminal sialic acid moiety of the hybrid-type glycan account for more than half of the buried surface area at the interface and contribute all the intermolecular hydrogen bonds. PG16 $Arg94_{LC}$ and $His95A_{LC}$ make three hydrogen bonds with the terminal sialic acid, and $Lys57_{HC}$ and $His59_{HC}$ contribute three. $Arg94_{LC}$ also has one hydrogen bond (3.9 Å) with the preceding galactose moiety of the glycan, which also has some stacking interactions with $Trp64_{HC}$ (Fig. 2e and Supplementary Table 2). This confirmed our previous paratope analysis of PG16 that revealed that mutation of $Trp64_{HC}$ to arginine affected neutralization[18]. Unlike $Asn160_{gp120}$-linked $Man_5GlcNAc_2$, in which six of seven saccharide rings contribute to the buried surface of the interface, the hybrid-type glycan at $Asn173_{gp120}$ makes contacts with the antibody through only four of the total ten saccharide rings. Of note, in the structure of PG9 bound to scaffolded V1–V2 ZM109, density could only be seen for the protein-proximal *N*-acetylglucosamine at position 173, with only one hydrogen bond with PG9. However, the structure of PG9 bound to scaffolded V1–V2 CAP45 showed multiple interactions with $Man_5GlcNAc_2$ at $Asn156_{gp120}$, the equivalent spatial position to $Asn173_{gp120}$. We also observed binding of PG9 to scaffolded V1–V2

grown in HEK293F cells in the presence of swainsonine (Supplementary Fig. 1a), and this indicates that PG9 may also bind hybrid-type glycan present in some sequences. The PG16 heavy-chain residues that interact with the sialic acid are equivalent in PG9 with $His59_{HC}$ and $Trp64_{HC}$, both obtained by somatic mutation[13,41]. However, the light-chain residues that interact with sialic acid and galactose in PG16 differ in PG9 ($Thr94_{LC}$ and $Arg95A_{LC}$ in PG16 compared to $Arg94_{LC}$ and $His95A_{lc}$ in PG9). These appear to preclude ideal interactions with the hybrid-type glycan, and this suggests that affinity maturation of a few light-chain residues may allow for recognition of hybrid-type and complex-type glycans (Fig. 3c).

It is notable that we only observed an α2–6–linked sialic acid on the hybrid-type glycan in the crystallized structure. Studies have shown that glycoproteins produced in HEK293 cells contain primarily α2–6 sialic acids, although α2–3 sialic acids are also present[42–45]. To confirm the presence of the sialic acid linkage observed in the crystal structure, we treated the scaffold 1FD6 V1–V2 ZM109 A4 with various neuraminidases that have different specificities for α2–3 and α2–6 sialic acids and evaluated binding to PG16 and PG9 by enzyme-linked immunosorbent assay (ELISA; Supplementary Fig. 2b and Supplementary Note). When scaffolded V1–V2 was treated with neuraminidase or sialidase A (which preferentially cleaves α2–6 sialic acids over α2–3), binding of PG16 was no longer observed, but when treated with α2–3 neuraminidase (which is highly selective for α2–3 sialic acids), binding to PG16 was retained. PG9 was less affected by neuraminidase treatment, although a preference of α2–6 sialosides was observed. These results indicate that an α2–6 sialic acid in the complex glycan is needed for PG16 binding.

NMR analysis of PG16 and PG9 recognition of glycan

To determine glycan recognition and binding-site selectivity for PG16 and PG9, we examined glycan binding by each antibody and by four antibody mutants designed to specifically knock out glycan recognition at individual sites. These included a PG16 $W64_{HC}R$ mutant that binds only N-glycan 160 ($PG16_{160}$), a PG16 $N100P_{HC}R$ mutant that binds only N-glycan 173 ($PG16_{173}$), a PG9 $S55_{HC}R$ mutant that binds only N-glycan 160 ($PG9_{160}$) and a PG9 $N100P_{HC}R$ mutant that binds only N-glycan 173 ($PG9_{173}$). By using saturation transfer difference (STD) NMR, we screened these antibodies for qualitative binding to commercially available glycans and relevant glycan fragments (Supplementary Fig. 3a), including biantennary complex type (a surrogate for hybrid type) and $Man_5GlcNAc_2$, and when binding was sufficiently strong we measured binding affinities. The NMR spectra showed that PG16 bound only two of the glycans tested, namely biantennary complex type (K_d = 1.26 ± 0.48 mM) and $Man_5GlcNAc_2$ (Fig. 3d). (We observed binding of $Man_5GlcNAc_2$, but the signal intensities were too weak for us to measure the K_d. This is probably because of the absence of hydrogen bonds that are present in PG9, especially at 100_{HC} and $100B_{HC}$ where aspartate-to-isoleucine and arginine-to-histidine variations occur in PG9 and PG16, respectively.) The biantennary complex–type glycan contains two terminal branches that are identical to the complex-type branch present in the hybrid-type glycan that makes most of the contacts with PG16, as shown in the crystal structure (Fig. 3). Hybrid-type glycans are not commercially available and therefore were not tested for binding. The STD spectrum of biantennary complex–type glycan in the

presence of PG16 showed very selective STD enhancements for protons of sialic acid and galactose; this suggests proximity of these residues to PG16 in the bound state (Fig. 3). These data are in agreement with the crystal structure, which showed that the major interactions between hybrid-type glycan and PG16 are mediated through the terminal sialic acid and preceding galactose ring. To confirm the role of sialic acid, we tested binding of PG16 to an asialocomplex-type glycan lacking the terminal sialic acid by STD NMR under identical conditions. In addition to the absence of the sialic acid signals, the signal intensities over the entire difference spectrum were markedly lower than those for the biantennary complex–type glycan. This indicates substantially weaker binding of PG16 to the asialocomplex–type glycan (Supplementary Fig. 3b, overlay of two STDs). Previously we reported that PG9 binds $Man_5GlcNAc_2$ with a K_d = 1.6 ± 0.91 mM by STD NMR[18], and although we observed binding of PG9 to complex-type glycans by NMR, the affinity was too weak to be measured.

We next analyzed binding of mutant PG9 and PG16 antibodies to $Man_5GlcNAc_2$ and biantennary complex–type glycans by using STD NMR. These mutant antibodies could bind only one site, N-glycan 160 or N-glycan 173. We used $Man_9GlcNAc_2$ as a control and did not observe binding for any of the antibodies. $PG16_{173}$ (mutated to bind N-glycan 173 only) bound complex-type glycan with a K_d of 1.19 + 0.45 mM, whereas we did not observe binding to $Man_5GlcNAc_2$; $PG16_{160}$ (mutated to bind only N-glycan 160) bound negligibly to $Man_5GlcNAc_2$ as well as to biantennary complex-type glycan (Fig. 4 and Supplementary Fig. 3c). PG9160 (mutated to bind only N-glycan 160) bound $Man_5GlcNAc_2$ with a K_d = 1.16 + 0.40 mM and did not show binding to biantennary complex-type glycan; $PG9_{173}$ (mutated to bind only N-glycan 173) showed very weak binding to biantennary complex-type glycan and to $Man_5GlcNAc_2$. However, the STD signal intensities were too weak to integrate accurately (Fig. 4 and Supplementary Fig. 3d). Nonetheless, qualitative comparison of the two STD spectra obtained under identical conditions showed that $PG9_{173}$ binds to biantennary complex-type glycan better than to $Man_5GlcNAc_2$ at this site (Supplementary Fig. 3d). PG16, therefore, binds preferentially to a complex-type glycan at $Asn173gp_{120}$. Unexpectedly, binding of PG16 to $Man_5GlcNAc_2$ at $Asn160gp_{120}$ was negligible in the NMR spectra even though $Man_5GlcNAc_2$ linked to Asn160 of V1-V2 contributes seven intermolecular hydrogen bonds and over 1,100 $Å^2$ of buried surface area at the PG16-V1-V2 interface. N-glycan 160 is also critical for neutralization[13]. The weaker affinity of PG16 for $Man_5GlcNAc_2$ at $Asn160_{gp120}$ compared to that of PG9 can be attributed to the lack of sufficient interactions between PG16 and the protein-proximal saccharide moiety of the glycan. The large buried surface area at the interface between $Man_5GlcNAc_2$ at $Asn160_{gp120}$ and PG16, as revealed in the crystal structure, however, suggests that PG16 recognizes $Man_5GlcNAc_2$ with a reasonable affinity only in the glycan-plus-peptide context. PG9, in contrast, binds preferentially to $Man_5GlcNAc_2$ at $Asn160_{gp120}$ but binds very weakly to complex-type glycan at $Asn173_{gp120}$.

A chimeric antibody, PG9-PG16-RSH

The structure revealed that recognition of complex-type N-linked glycan by PG16 involves three residues in the light chain ($Arg94_{LC}$, $Ser95_{LC}$ and $His95A_{lc}$), two of which were obtained through somatic hypermutation from germ line (from $Ser94_{LC}$ and $Thr95A_{LC}$;

Figs. 2 and 5). In PG9, the equivalent residues are $Thr94_{LC}$, $Arg95_{LC}$ and $Arg95A_{LC}$. We created a chimeric antibody (PG9-16-RSH) that combines PG9's recognition of the V1–V2 side chain and the high-mannose N-glycan 160 with PG16's recognition of hybrid-type or complex-type glycans by substituting Arg94, Ser95 and His95A from the PG16 light chain into the light chain of PG9. Subsequently, the binding affinities of the chimeric antibody PG9-16-RSH with $Man_5GlcNAc_2$ or biantennary complex–type glycan were determined through single ligand–titration STD NMR experiments. The K_d values obtained were 1.57 ± 0.41 mM and 1.34 ± 0.35 mM for $Man_5GlcNAc_2$ and biantennary complex–type glycan, respectively (Fig. 5 and Supplementary Fig. 3e). When compared to the affinity of PG9 for $Man_5GlcNAc_2$ (1.60 ± 0.91 mM) and the affinity of PG16 for biantennary complex–type glycan (1.26 ± 0.48 mM), these results suggest that the chimeric antibody preserves the glycan specificity of the individual antibodies when their corresponding recognition elements are combined in a single antibody.

To evaluate whether the improved glycan binding by the chimeric antibody would lead to improved HIV-1 neutralization properties, we performed neutralization assays in triplicate with 21 different HIV-1 strains. We observed a roughly three-fold improvement in neutralization for the chimeric antibody PG9-16-RSH compared to PG9 (50% inhibitory concentration, IC_{50}; Fig. 6a). However, we observed strain-to-strain variation: PG9-16-RSH showed improved potency compared to PG9 on 17 viruses, with a median fold improvement of 4.6; no improvement on two viruses; and decreased potency on two viruses. Notably, the more substantial effects were observed with strains that were already neutralized potently by PG9 (Fig. 6b and Supplementary Table 3): for the eight strains with PG9 $IC_{50} < 0.05$, the median improvement in IC_{50} for PG9-16-RSH as compared to PG9 was five-fold; three of the four strains with PG9 $IC_{50} > 5$ showed a modest decrease in potency. Overall, PG9-16-RSH showed no increase in breadth relative to PG9. We also tested neutralization by PG9-16-RSH, PG9 and PG16 in a large panel (195 viruses described previously)[18] (Supplementary Table 3) and generated breadth/potency curves (Fig. 6c). We generated an optimal PG9 and PG16 curve by taking the lower IC_{50} between PG9 and PG16 for each HIV-1 isolate (MIN(PG9-IC_{50},PG16-IC_{50})) and comparing it to the PG9-16-RSH breadth/potency curve (Fig. 6c). Notably, the PG9-16-RSH curve and the (MIN(PG9-IC_{50},PG16-IC_{50})) curve almost completely superposed (Fig. 6c).

Because the enhanced glycan recognition of PG9-PG16-RSH may lead to reactivity with glycans on self proteins, we tested the chimera along with the parent PG9 and PG16 for autoreactivity (Supplementary Fig. 4). PG9-16-RSH retained the clean autoreactivity profile of the parent PG9 and PG16 antibodies (Supplementary Fig. 4). Overall, our results demonstrate how the combination of optimal features of recognition between somatically related antibodies can lead to enhanced neutralization of HIV-1.

Role of sialic acid in HIV-1 neutralization by PG9-16-RSH

In the preceding sections, structural and STD NMR analyses show that PG16 binds a complex-type or hybrid-type N-glycan through its terminal sialic acid and preceding galactose moiety. To further investigate the role of the terminal sialic acid on complex-type glycan on the viral spike, we performed HIV-1 neutralization assays with and without

treating viruses with neuraminidase, an enzyme that cleaves the glycosidic linkage between sialic acid and galactose. We chose three HIV-1 strains (AC10, Q769.h5 and ZM176), for which the PG9-16-RSH chimera showed at least a five-fold improvement in potency over PG9. PG16 and PG9-16-RSH were less potent against neuraminidase-treated viruses than against untreated viruses, exhibiting 2-30 times higher IC_{50} values (Fig. 7). PG9 neutralization was less affected by the neuraminidase treatment (two times higher IC_{50}). This decreased neutralization of neuraminidase-treated viruses by PG16 and PG9-16-RSH confirms the role of hybrid-type or complex-type glycan at $Asn156_{gp120}$ or $Asn173_{gp120}$ and the terminal sialic acid moiety in the recognition of gp120 by PG16. PG16 and PG9-16-RSH are more potent when the sialic acid on hybrid-or complex-type N-linked glycans are present on the viral spike, and this raises the question of which glycan types are on the viral spike. Of note, the neuraminidase-treated viruses were still neutralized by PG16 and PG9-16-RSH (at a lower potency), and this indicates that other interactions, including those with V1–V2 residues and with $Man_5GlcNAc_2$ at N-glycan 160 and weak interactions with the galactose moiety of N-glycan 173, were sufficient for neutralization. Indeed, a few viruses do not possess a glycan at position 156 or 173 but are neutralized by both PG9 and PG16, and this indicates that this glycan is not necessary for effective neutralization by these antibodies. Nevertheless, the reduced potency after neuraminidase treatment suggests that interaction with sialic acid is an important contributor to overall binding strength.

Discussion

Somatic variation represents a general antibody mechanism to enhance affinity and overcome viral diversity[5,37,46–48]. In the case of the PG9 and PG16 antibodies, the combination of PG9 and PG16 neutralizes HIV-1 with better breadth (PG9) and potency (PG16) than for either antibody alone (Fig. 6c). Here we used both crystallographic and NMR techniques to elucidate the structural basis for the neutralization differences between PG9 and PG16 and to create a PG9-16 variant with the ability to neutralize and determine the optimal PG9-PG16 combination.

Can our results with PG9 and PG16 be extended to other antibodies? Our analysis identifies critical contact residues that differ between somatic relatives, and it makes use of somatic variation to design antibodies with enhanced function. Such analysis would probably have identified the important $G54W_{HC}$ alteration, which increases the potency of antibody NIH45-46 by approximately ten times[48]; Trp54 is at a critical contact between antibody and gp120, and a tryptophan is naturally present in the VRC03 antibody[47,49], a somatic relative of NIH45-46. Meanwhile, analysis of the somatic variation for various gp120 glycan–reactive antibodies shows that a number of somatic variants occur at glycan-interactive residues (Supplementary Fig. 5). Our results suggest that a complex-type N-linked glycan often exists at 173_{gp120} or 156_{gp120}. This may in part explain observations regarding the presence and importance of complex glycans on the viral spike. Differences have been observed in potency between various neutralization assays[50] as well as in the amount and types of glycans present on viruses from different sources[24]. In the case of glycopeptide-directed antibodies, such as PG9 and PG16, antibody neutralization assays should be re-evaluated to take into account the *in vivo* diversity of glycans on the functional viral spike (especially at Asn156 or Asn173), as this may more accurately reflect the breadth and/or

potency of these antibodies[51]. PG9 and PG16 both require $Man_5GlcNAc_2$ at position 160_{gp120} to neutralize HIV-1 (ref. 13), whereas the N-linked glycan at position 156 or 173, although usually present in most viruses, is not required[18]. Overall, we have defined the structural basis for recognition of diverse glycans at the $Asn156_{gp120}$ or $Asn173_{gp120}$ site by antibodies PG9 and PG16 (Fig. 8).

Our results, along with the structure of PGT121 bound to a complex-type glycan[37], represent some of the first reports of an HIV-1–neutralizing antibody whose epitope comprises a terminal sialic acid–containing glycan. Sialic acid is atypical in terms of its carbohydrate chemistry: it is a C9 sugar with a C-2 anomeric carbon, a carboxylate at C-1, an amine at C-5 and a glycerol side chain at C-7 to C-9. Accordingly, sialic acid–binding proteins, such as the Siglec family and the selectins, have developed precise ways of recognizing and binding to this unique sugar[52,53]. This is best illustrated in the Siglecs, in which the glycerol side chain and N-acetyl group of sialic acid hydrogen-bond to main chain atoms, to precisely mimic an extended antiparallel β-sheet, and a conserved arginine forms hydrogen bonds to the C-1 carboxylate[54]. For PG16, the immune system appears to have evolved a different strategy for sialic acid recognition in which backbone and side chain nitrogens of two histidine residues, one located in the heavy chain and one in the light chain of the antibody, dominate the electrostatic interactions. Although arginine residues are present, direct interactions between their guanidine groups and sialic acid are (somewhat unexpectedly) not observed.

In terms of vaccine design, our data indicate that design efforts for V1–V2–containing immunogens will probably need to take into account specific glycans at two different sites; a gp120-based immunogen targeting this region should probably have a $Man_5GlcNAc_2$ at residue $160_{immunogen}$ and a complex-type glycan at residue $156_{immunogen}$ or $173_{immunogen}$. Testing of heterogeneously glycosylated immunogens, in which multiple permutations of glycan type and glycosylation site have been introduced into a given V1–V2 sequence, may provide a means to confirm this hypothesis. In general, it is notable that, whereas variation can be observed at N-glycan 156 or 173 sites, our data support the presence of a $Man_5GlcNAc_2$ at position 160. An understanding of the factors that lead to conservation at N-glycan 160 and diversity at N-glycan 156 or 173 may assist in understanding the interplay between viral glycan diversity and antibody-mediated recognition and neutralization.

Online Methods

Formation and purification of PG16–V1–V2 scaffold complexes

Expression and purification of 1FD6 V1–V2 scaffolds and PG16 N23Q HRV3C were performed as described previously[18]. Briefly, the genes coding for the scaffolded V1–V2 were transiently transfected in HEK293S GnTI$^-$ cells and HEK293F in which 10 mg of swainsonine had been added 2 h before transfection. Supernatants were collected after 4–5 days, and the scaffolded V1–V2 proteins were purified over a Ni column, the tags cleaved with HRV3C and the samples run over gel-filtration columns. Complexes were formed as described previously, with a PG16 N23Q HRV3C IgG on-column procedure with 30-fold molar excess of the V1–V2 scaffold[18]. The yield of complex obtained was low, ∼2%.

PG16–V1–V2 complex crystallization and data collection

A complex of PG16 bound to 1FD6ZM109 with four N-linked asparagines mutated to alanine (except Asn160 and Asn173) was screened against 576 crystallization conditions by a Cartesian Honeybee crystallization robot. Initial crystals were grown by the vapor diffusion method in sitting drops at 20 °C by mixing 0.2 μl of protein complex with 0.2 μl of reservoir solution (15% (w/v) PEG 3350, 20% (v/v) isopropanol and 0.2 M ammonium citrate, pH 7.5). Crystals suitable for diffraction were manually reproduced in hanging drops by mixing equal volumes of protein complex with reservoir solution (15% (w/v) PEG 3350, 20% (v/v) isopropanol and 0.2 M ammonium citrate, pH 7.5). Single crystals were flash frozen in liquid nitrogen in 25% (w/v) PEG 3350, 34% (v/v) isopropanol, 0.2 M ammonium citrate, pH 7.5, and 15% (v/v) 2*R*,3*R*-butanediol. Data to 2.50 Å were collected at a wavelength of 1.00 Å at the SER-CAT beamline ID-22 (Advanced Photon Source, Argonne National Laboratory).

PG16–V1–V2 complex structure determination and refinement

The diffraction data were processed with the HKL2000 suite[55]. The PG9-1FD6ZM109 structure was used as the search model for the PG16-1FD6ZM109 data set. A molecular replacement solution consisting of one complex per asymmetric unit was obtained by Phenix[56]. Coot[57] and Phenix[58] were used for model building and refinement, respectively. Final data collection and refinement statistics are presented in Table 1. The Ramachandran plot as determined by MolProbity[59] shows 95.1% of all residues in favored regions and 99.8% of all residues in allowed regions. The coordinates were deposited in the PDB under PDB ID 4DQO.

NMR experiments

NMR data were acquired on a Bruker Avance 600 MHz NMR equipped with a triple-resonance cryoprobe with *z*-axis gradients. Topspin 2.1 was used to process and analyze the NMR data. Resonance assignments of the glycans were made by 2D ^{1}H-^{13}C correlation spectra including HSQC, HSQC-TOCY and HSQC-NOESY experiments using standard pulse sequences (Supplementary Table 4). 1D STD NMR spectra were obtained by applying a train of 50-ms Gaussian-shaped radio-frequency pulses separated by 1-ms delays for a total of 0.2-s saturation time with the carrier set at −1 p.p.m. (to selectively irradiate protein resonances), or +40 p.p.m. for reference spectra. Difference spectra were obtained by subtracting the reference spectrum from the saturated spectrum. Each was acquired with 2,048 scans giving an average experiment time of 8 h. During NMR experiments, water and protein resonances were suppressed by a binomial 3-9-19 pulse sequence and a 10-ms T1ρ filter, respectively. Samples were prepared in 20 mM sodium phosphate buffer containing 50 mM sodium chloride at pH 6.8. The equilibrium dissociation constants (K_d) of glycans were measured by fitting ASTD values as a function of glycan concentration using the equation $y=B_{max}/(K_d+x)$, where x is the ligand concentration and B_{max} represents the plateau of the curve. Experiments were carried out at 298 K.

Neutralization assays

Neutralization was measured by using single-round-of-infection HIV-1 Env-pseudoviruses and TZM-bl target cells, as described previously[49,60,61]. Neutralization curves were fit by nonlinear regression by a five-parameter Hill slope equation as previously described[60]. The 50% and 80% inhibitory concentrations (IC_{50} and IC_{80}) were reported as the antibody concentrations required to inhibit infection by 50% and 80%, respectively. For the sialic acid experiments, unconcentrated pseudoviruses were either treated or mock treated with 75 mU of neuraminidase (Sigma-Aldrich, cat. no. N8271) at 37 °C for 4 h before addition of the antibodies.

Autoreactivity assays

Reactivity to HIV-1 negative human epithelial (HEp-2) cells was determined by indirect immunofluorescence on slides, with Evans Blue as a counterstain and FITC-conjugated goat anti-human IgG (Zeus Scientific)[62]. Slides were photographed on a Nikon Optiphot fluorescence microscope. Kodachrome slides were taken of each monoclonal antibody binding to HEp-2 cells at a10-s exposure and the slides scanned into digital format (Supplementary Fig. 4). The Luminex AtheNA Multi-Lyte ANA test (Wampole Laboratories) was used to test for monoclonal antibody reactivity to SSA/Ro, SS-B/La, Sm, ribonucleoprotein (RNP), Jo-1, double-stranded DNA, centromere B and histone and was performed per the manufacturer's specifications and as previously described[62]. Monoclonal antibody concentrations assayed were 50, 25, 12.5 and 6.25 μg/ml. Ten milliliters for each concentration were incubated with the Luminex fluorescent beads and the test performed per the manufacturer's specifications. Reactivity with cardiolipin was tested with Luminex technology as well, with the ACL assay (Wampole Laboratories).

ELISAs

For details on the assays used to measure binding of PG9 and PG16 or of lectins to scaffolded V1–V2 (Supplementary Figs. 1 and 2), please see Supplementary Note.

Figures

Structure figures were prepared with PyMol (http://www.pymol.org/).

Supplementary Material

Refer to Web version on PubMed Central for supplementary material.

Acknowledgments

We thank J. Stuckey for assistance with figures and members of the Structural Biology Section and Structural Bioinformatics Core, Vaccine Research Center for discussions or comments on the manuscript; A. Kumar for sharing the ELISA binding protocol with biotinylated lectins; P. Azadi and S. Archer-Hartmann, University of Georgia, for performing glycan analyses and glycopeptide mapping; J. Baalwa (Department of Pathology, University of Alabama at Birmingham, Birmingham, Alabama, USA), D. Ellenberger (International Laboratory Branch, Division of Global HIV/AIDS, Center for Global Health, Centers for Disease Control and Prevention, Atlanta, Georgia, USA), D. Gabuzda (Department of Cancer Immunology and AIDS, Dana-Farber Cancer Institute, Boston, Massachusetts, USA), F. Gao (Duke Human Vaccine Institute, Duke University Medical Center, Durham, North Carolina, USA), B. Hahn (Department of Pathology, University of Alabama at Birmingham, Birmingham, Alabama, USA), K. Hong (State Key Laboratory for Infectious Disease Control and Prevention, National Center for

AIDS/STD Control and Prevention, Chinese Center for Disease Control and Prevention, Beijing, China), J. Kim (US Military HIV Research Program, Henry M. Jackson Foundation, Bethesda, Maryland, USA), F. McCutchan (US Military HIV Research Program, Henry M. Jackson Foundation, Bethesda, Maryland, USA), D. Montefiori (Department of Surgery, Duke University, Durham, North Carolina, USA), L. Morris, (Centre for HIV and STIs, National Institute for Communicable Diseases, Johannesburg, South Africa), J. Overbaugh (Program for Appropriate Technology in Health, Seattle, Washington, USA), E. Sanders-Buell (US Military HIV Research Program, Henry M. Jackson Foundation, Bethesda, Maryland, USA), G. Shaw (Department of Pathology, University of Alabama at Birmingham, Birmingham, Alabama, USA), R. Swanstrom (University of North Carilina Center for AIDS Research, University of North Carolina at Chapel Hill, Chapel Hill, North Carolina, USA), M. Thomson (University of Birmingham, Birmingham, UK), S. Tovanabutra (Department of Retrovirology, Armed Forces Research Institute of Medical Sciences, Bangkok, Thailand), C. Williamson (Institute of Infectious Diseases and Molecular Medicine, Division of Medical Virology, University of Cape Town and National Health Laboratory Services, Cape Town, South Africa) and L. Zhang (Department of Public Health, Center for Disease Control and Prevention in Jiangxi Province, Nanchang, China) contributing the HIV-1 Envelope plasmids used in our neutralization panel. Support for this work was provided by the US National Institutes of Health Intramural Research Programs (Vaccine Research Center, National Institute of Allergy and Infectious Diseases, and the National Institute of Diabetes and Digestive and Kidney Diseases), by grants from the International AIDS Vaccine Initiative's Neutralizing Antibody Consortium and by the Center for HIV AIDS Vaccine Immunology Grant AI 5U19 AI 067854-06 from the US National Institutes of Health (J.E., K.E.L., J.B., S.M.A. and B.F.H.), by US National Institutes of Health grant 1R21 AI101035 (M.N.A. and L-X.W.) and by the US National Institutes of Health (NIH/NCRR)-funded grant P41 RR018502-01 to the Complex Carbohydrate Research Center. Use of sector 22 (Southeast Region Collaborative Access team) at the Advanced Photon Source was supported by the US Department of Energy, Basic Energy Sciences, Office of Science under contract number W-31-109-Eng-38.

References

1. Pantophlet R, Burton DR. GP120: target for neutralizing HIV-1 antibodies. Annu Rev Immunol. 2006; 24:739–769. [PubMed: 16551265]
2. Wyatt R, Sodroski J. The HIV-1 envelope glycoproteins: fusogens, antigens, and immunogens. Science. 1998; 280:1884–1888. [PubMed: 9632381]
3. Binley JM, et al. Analysis of the interaction of antibodies with a conserved enzymatically deglycosylated core of the HIV type 1 envelope glycoprotein 120. AIDS Res Hum Retroviruses. 1998; 14:191–198. [PubMed: 9491908]
4. Walker LM, et al. A limited number of antibody specificities mediate broad and potent serum neutralization in selected HIV-1 infected individuals. PLoS Pathog. 2010; 6:e1001028. [PubMed: 20700449]
5. Walker LM, et al. Broad neutralization coverage of HIV by multiple highly potent antibodies. Nature. 2011; 477:466–470. [PubMed: 21849977]
6. Kwong PD, et al. Structure of an HIV gp120 envelope glycoprotein in complex with the CD4 receptor and a neutralizing human antibody. Nature. 1998; 393:648–659. [PubMed: 9641677]
7. Wyatt R, et al. The antigenic structure of the HIV gp120 envelope glycoprotein. Nature. 1998; 393:705–711. [PubMed: 9641684]
8. Trkola A, et al. Human monoclonal antibody 2G12 defines a distinctive neutralization epitope on the gp120 glycoprotein of human immunodeficiency virus type 1. J Virol. 1996; 70:1100–1108. [PubMed: 8551569]
9. Sanders RW, et al. The mannose-dependent epitope for neutralizing antibody 2G12 on human immunodeficiency virus type 1 glycoprotein gp120. J Virol. 2002; 76:7293–7305. [PubMed: 12072528]
10. Scanlan CN, et al. The broadly neutralizing anti-human immunodeficiency virus type 1 antibody 2G12 recognizes a cluster of α1→2 mannose residues on the outer face of gp120. J Virol. 2002; 76:7306–7321. [PubMed: 12072529]
11. Binley JM, et al. Profiling the specificity of neutralizing antibodies in a large panel of plasmas from patients chronically infected with human immunodeficiency virus type 1 subtypes B and C. J Virol. 2008; 82:11651–11668. [PubMed: 18815292]
12. Walker LM, et al. Rapid development of glycan-specific, broad, and potent anti-HIV-1 gp120 neutralizing antibodies in an R5 SIV/HIV chimeric virus infected macaque. Proc Natl Acad Sci USA. 2011; 108:20125–20129. [PubMed: 22123961]

13. Walker LM, et al. Broad and potent neutralizing antibodies from an African donor reveal a new HIV-1 vaccine target. Science. 2009; 326:285–289. [PubMed: 19729618]
14. Calarese DA, et al. Dissection of the carbohydrate specificity of the broadly neutralizing anti-HIV-1 antibody 2G12. Proc Natl Acad Sci USA. 2005; 102:13372–13377. [PubMed: 16174734]
15. Calarese DA, et al. Antibody domain exchange is an immunological solution to carbohydrate cluster recognition. Science. 2003; 300:2065–2071. [PubMed: 12829775]
16. Doores KJ, Fulton Z, Huber M, Wilson IA, Burton DR. Antibody 2G12 recognizes di-mannose equivalently in domain- and nondomain-exchanged forms but only binds the HIV-1 glycan shield if domain exchanged. J Virol. 2010; 84:10690–10699. [PubMed: 20702629]
17. Wang LX, Ni J, Singh S, Li H. Binding of high-mannose-type oligosaccharides and synthetic oligomannose clusters to human antibody 2G12: implications for HIV-1 vaccine design. Chem Biol. 2004; 11:127–134. [PubMed: 15113002]
18. McLellan JS, et al. Structure of HIV-1 gp120 V1/V2 domain with broadly neutralizing antibody PG9. Nature. 2011; 480:336–343. [PubMed: 22113616]
19. Pejchal R, et al. A potent and broad neutralizing antibody recognizes and penetrates the HIV glycan shield. Science. 2011; 334:1097–1103. [PubMed: 21998254]
20. Sattentau QJ. Vaccinology: a sweet cleft in HIV's armour. Nature. 2011; 480:324–325. [PubMed: 22170674]
21. Leonard CK, et al. Assignment of intrachain disulfide bonds and characterization of potential glycosylation sites of the type 1 recombinant human immunodeficiency virus envelope glycoprotein (gp120) expressed in Chinese hamster ovary cells. J Biol Chem. 1990; 265:10373–10382. [PubMed: 2355006]
22. Mizuochi T, et al. Carbohydrate structures of the human-immunodeficiency-virus (HIV) recombinant envelope glycoprotein gp120 produced in Chinese-hamster ovary cells. Biochem J. 1988; 254:599–603. [PubMed: 2845957]
23. Zhu X, Borchers C, Bienstock RJ, Tomer KB. Mass spectrometric characterization of the glycosylation pattern of HIV-gp120 expressed in CHO cells. Biochemistry. 2000; 39:11194–11204. [PubMed: 10985765]
24. Bonomelli C, et al. The glycan shield of HIV is predominantly oligomannose independently of production system or viral clade. PLoS ONE. 2011; 6:e23521. [PubMed: 21858152]
25. Doores KJ, et al. Envelope glycans of immunodeficiency virions are almost entirely oligomannose antigens. Proc Natl Acad Sci USA. 2010; 107:13800–13805. [PubMed: 20643940]
26. Eggink D, et al. Lack of complex N-glycans on HIV-1 envelope glycoproteins preserves protein conformation and entry function. Virology. 2010; 401:236–247. [PubMed: 20304457]
27. Go EP, et al. Characterization of glycosylation profiles of HIV-1 transmitted/founder envelopes by mass spectrometry. J Virol. 2011; 85:8270–8284. [PubMed: 21653661]
28. Pabst M, Chang M, Stadlmann J, Altmann F. Glycan profiles of the 27 N-glycosylation sites of the HIV envelope protein CN54gp140. Biol Chem. 2012; 393:719–730. [PubMed: 22944675]
29. Mizuochi T, et al. Diversity of oligosaccharide structures on the envelope glycoprotein gp 120 of human immunodeficiency virus 1 from the lymphoblastoid cell line H9. Presence of complex-type oligosaccharides with bisecting *N*-acetylglucosamine residues. J Biol Chem. 1990; 265:8519–8524. [PubMed: 2341393]
30. Kong L, et al. Expression-system-dependent modulation of HIV-1 envelope glycoprotein antigenicity and immunogenicity. J Mol Biol. 2010; 403:131–147. [PubMed: 20800070]
31. Binley JM, et al. Role of complex carbohydrates in human immunodeficiency virus type 1 infection and resistance to antibody neutralization. J Virol. 2010; 84:5637–5655. [PubMed: 20335257]
32. Ouellet M, et al. Galectin-1 acts as a soluble host factor that promotes HIV-1 infectivity through stabilization of virus attachment to host cells. J Immunol. 2005; 174:4120–4126. [PubMed: 15778371]
33. St-Pierre C, et al. Host-soluble galectin-1 promotes HIV-1 replication through a direct interaction with glycans of viral gp120 and host CD4. J Virol. 2011; 85:11742–11751. [PubMed: 21880749]

34. van Montfort T, et al. HIV-1 N-glycan composition governs a balance between dendritic cell-mediated viral transmission and antigen presentation. J Immunol. 2011; 187:4676–4685. [PubMed: 21957147]
35. Reitter JN, Means RE, Desrosiers RC. A role for carbohydrates in immune evasion in AIDS. Nat Med. 1998; 4:679–684. [PubMed: 9623976]
36. Wei X, et al. Antibody neutralization and escape by HIV-1. Nature. 2003; 422:307–312. [PubMed: 12646921]
37. Mouquet H, et al. Complex-type N-glycan recognition by potent broadly neutralizing HIV antibodies. Proc Natl Acad Sci USA. 2012; 109:E3268–E3277. [PubMed: 23115339]
38. Bonsignori M, et al. Analysis of a clonal lineage of HIV-1 envelope V2/V3 conformational epitope-specific broadly neutralizing antibodies and their inferred unmutated common ancestors. J Virol. 2011; 85:9998–10009. [PubMed: 21795340]
39. Doores KJ, Burton DR. Variable loop glycan dependency of the broad and potent HIV-1-neutralizing antibodies PG9 and PG16. J Virol. 2010; 84:10510–10521. [PubMed: 20686044]
40. Kabat, EA.; Wu, TT.; Perry, HM.; Gottesman, KS.; Foeller, C. Sequences of Proteins of Immunological Interest. U.S. Department of Health and Human Services, National Institutes of Health 1991;
41. Pancera M, et al. Crystal structure of PG16 and chimeric dissection with somatically related PG9: structure-function analysis of two quaternary-specific antibodies that effectively neutralize HIV-1. J Virol. 2010; 84:8098–8110. [PubMed: 20538861]
42. Otto VI, Schurpf T, Folkers G, Cummings RD. Sialylated complex-type N-glycans enhance the signaling activity of soluble intercellular adhesion molecule-1 in mouse astrocytes. J Biol Chem. 2004; 279:35201–35209. [PubMed: 15201278]
43. Sánchez -Felipe L, Villar E, Munoz-Barroso I. α2–3- and α2–6- N-linked sialic acids allow efficient interaction of Newcastle Disease Virus with target cells. Glycoconj J. 2012; 29:539–549. [PubMed: 22869099]
44. Guo Y, et al. Analysis of hemagglutinin-mediated entry tropism of H5N1 avian infuenza. Virol J. 2009; 6:39. [PubMed: 19341465]
45. Durocher Y, Butler M. Expression systems for therapeutic glycoprotein production. Curr Opin Biotechnol. 2009; 20:700–707. [PubMed: 19889531]
46. Scheid JF, et al. Sequence and structural convergence of broad and potent HIV antibodies that mimic CD4 binding. Science. 2011; 333:1633–1637. [PubMed: 21764753]
47. Wu X, et al. Focused evolution of HIV-1 neutralizing antibodies revealed by structures and deep sequencing. Science. 2011; 333:1593–1602. [PubMed: 21835983]
48. Zhu J, et al. Somatic populations of PGT135–137 HIV-1-neutralizing antibodies identified by 454 pyrosequencing and bioinformatics. Front Microbiol. 2012; 3:315. [PubMed: 23024643]
49. Wu X, et al. Rational design of envelope identifies broadly neutralizing human monoclonal antibodies to HIV-1. Science. 2010; 329:856–861. [PubMed: 20616233]
50. Heyndrickx L, et al. International network for comparison of HIV neutralization assays: the NeutNet report II. PLoS ONE. 2012; 7:e36438. [PubMed: 22590544]
51. Euler Z, et al. Activity of broadly neutralizing antibodies, including PG9, PG16, and VRC01, against recently transmitted subtype B HIV-1 variants from early and late in the epidemic. J Virol. 2011; 85:7236–7245. [PubMed: 21561918]
52. May AP, Robinson RC, Vinson M, Crocker PR, Jones EY. Crystal structure of the N-terminal domain of sialoadhesin in complex with 3′ sialyllactose at 1.85 A resolution. Mol Cell. 1998; 1:719–728. [PubMed: 9660955]
53. Somers WS, Tang J, Shaw GD, Camphausen RT. Insights into the molecular basis of leukocyte tethering and rolling revealed by structures of P- and E-selectin bound to SLe(X) and PSGL-1. Cell. 2000; 103:467–479. [PubMed: 11081633]
54. Zhuravleva MA, Trandem K, Sun PD. Structural implications of Siglec-5-mediated sialoglycan recognition. J Mol Biol. 2008; 375:437–447. [PubMed: 18022638]
55. Otwinowski Z, Minor W. Processing of X-ray diffraction data collected in oscillation mode. Methods Enzymol. 1997; 276:307–326.

56. McCoy AJ, et al. Phaser crystallographic software. J Appl Crystallogr. 2007; 40:658–674. [PubMed: 19461840]
57. Emsley P, Cowtan K. Coot: model-building tools for molecular graphics. Acta Crystallogr D Biol Crystallogr. 2004; 60:2126–2132. [PubMed: 15572765]
58. Adams PD, et al. PHENIX: building new software for automated crystallographic structure determination. Acta Crystallogr D Biol Crystallogr. 2002; 58:1948–1954. [PubMed: 12393927]
59. Davis IW, et al. MolProbity: all-atom contacts and structure validation for proteins and nucleic acids. Nucleic Acids Res. 2007; 35:W375–W383. [PubMed: 17452350]
60. Li M, et al. Human immunodeficiency virus type 1 env clones from acute and early subtype B infections for standardized assessments of vaccine-elicited neutralizing antibodies. J Virol. 2005; 79:10108–10125. [PubMed: 16051804]
61. Seaman MS, et al. Multiclade human immunodeficiency virus type 1 envelope immunogens elicit broad cellular and humoral immunity in rhesus monkeys. J Virol. 2005; 79:2956–2963. [PubMed: 15709015]
62. Haynes BF, et al. Cardiolipin polyspecific autoreactivity in two broadly neutralizing HIV-1 antibodies. Science. 2005; 308:1906–1908. [PubMed: 15860590]

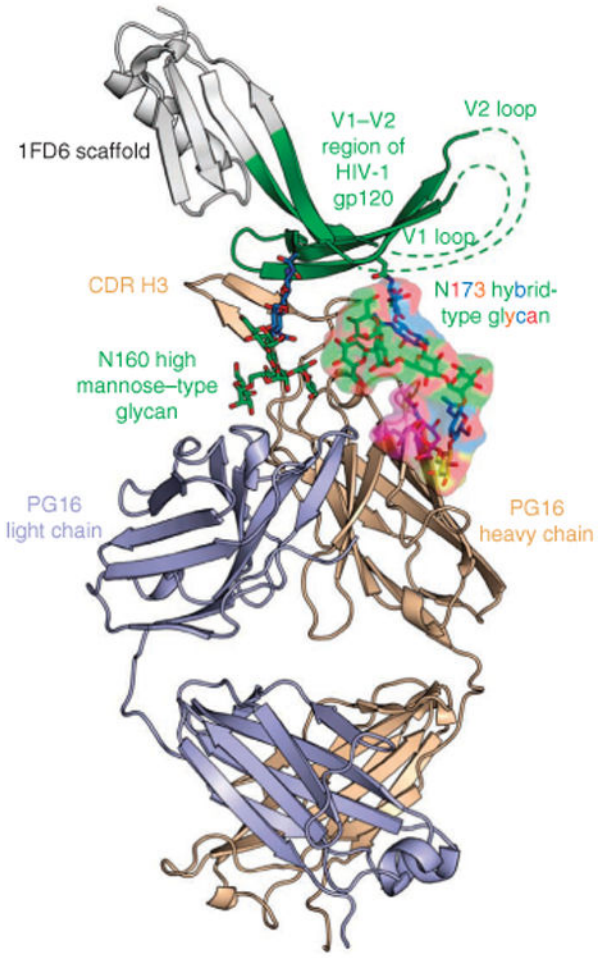

Figure 1.

Cocrystal structure of human antibody PG16 and scaffolded-V1–V2 of HIV-1 gp120 with a high mannose–type N-linked glycan at residue 160_{gp120} and a hybrid-type N-linked glycan at residue 173_{gp120}. The Fab of antibody PG16 (tan for heavy chain and light blue for light chain) along with V1–V2 (green) and 1FD6 scaffold (gray) are shown in ribbon representation. N-linked glycans (N) at residues 160 and 173 of V1–V2 are displayed in stick representation, with oxygen atoms in red and carbon atoms colored according to saccharide-subunit standard coloring (blue, *N*-acetylglucosamine; green, mannose; yellow, galactose; magenta, sialic acid). The hybrid-type glycan at residue 173 is highlighted with a partially transparent surface colored the same as underlying atoms.

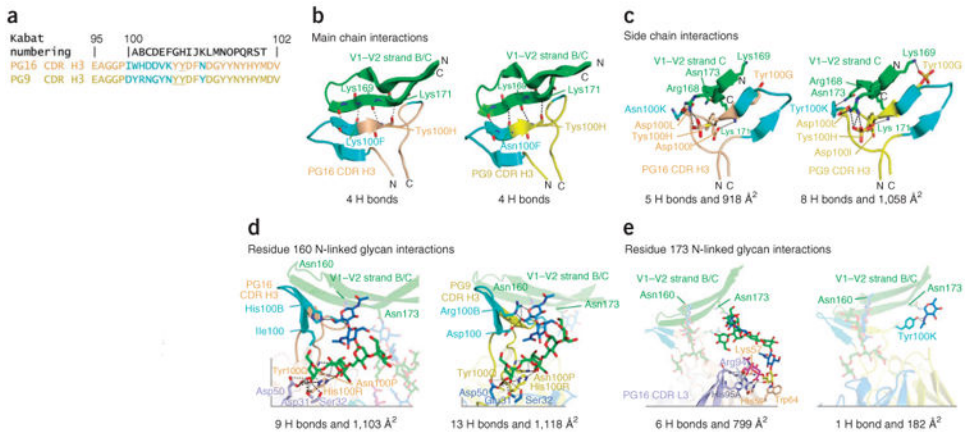

Figure 2.

PG16 and PG9 interactions with V1–V2 domain of HIV-1 gp120. Cocrystal structures of PG16 and PG9 bound to V1–V2 allow the relative strength of interactions to be compared. (**a**) PG16 and PG9 CDR H3 sequences based on Kabat numbering. Sequence differences are shown in cyan; sulfated tyrosines are underlined. (**b,c**) Sequence-independent, electrostatic main chain (**b**) and side chain (**c**) interactions of PG16 (left) and PG9 (right) with V1–V2 domain from strain ZM109. Ribbon representation of V1–V2 (green) and PG16 (tan) or PG9 (yellow) CDR H3s. Cyan, sequence-variable region of CDR H3s, as in **a**. (**d,e**) Sequence-independent glycan-mediated $Asn160_{gp120}$ glycan ($Man_5GlcNAc_2$) (**d**) and $Asn173_{gp120}$ glycan (complex-type) (**e**) interactions of PG16 (left) and PG9 (right) with V1–V2 domain from strain ZM109. Ribbon representation of V1–V2 (green), PG16-heavy chain (tan), PG16-light chain (light blue), PG9-heavy chain (yellow) and PG9-light chain (blue). Complex-type glycan and $Man_5GlcNAc_2$ are displayed as sticks and are color coded as in Figure 1. Antibody residues involved in hydrogen bonds to glycans are shown in sticks. Saccharide subunits are colored as in Figure 1. Intermolecular hydrogen bonds and electrostatic interactions are displayed by black (<3.5 Å) or gray (>3.5 Å). The number of hydrogen bonds (<3.5 Å) and the buried surface area for each interface are shown.

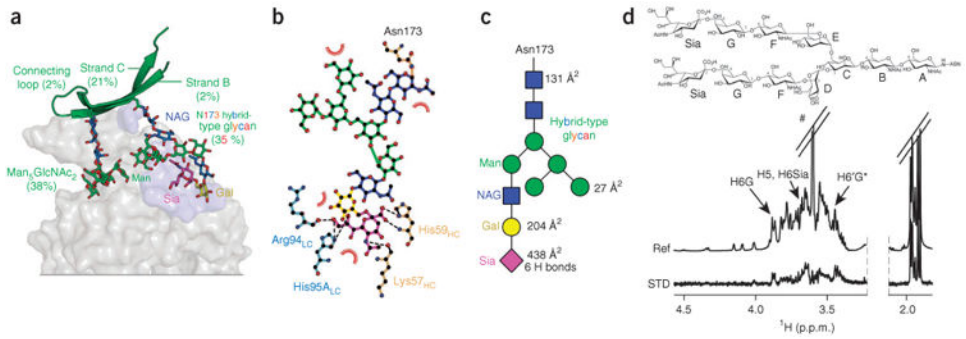

Figure 3.

PG16 interactions with hybrid-type N-linked glycan at residue 156_{gp120} or 173_{gp120}. (**a**) Paratope-epitope interface highlighting N-glycan 156_{gp120} or 173_{gp120}. PG16 is shown as a gray surface with the N-glycan 156_{gp120} or 173_{gp120} glycan-contact surface colored light blue. The contribution of each component of V1–V2 to the total buried surface is indicated. Saccharide subunits are colored as in Figure 1. NAG, *N*-acetylglucosamine; Man, mannose; Gal, galactose; Sia, sialic acid. (**b**) Ligplot showing hydrogen bonds (<3.5 Å) and hydrophobic interactions of hybrid-type glycan with PG16 heavy (tan) and light (light blue) chains. (**c**) Schematics of hybrid-type glycan showing the contribution of each saccharide ring to the PG16-glycan interfacial buried surface and the number of intermolecular hydrogen bonds (<3.5 Å) made by each ring. (**d**) Top, complex-type carbohydrate shown schematically with each pyranose ring labeled A–G and sialic acid labeled as Sia. Bottom, STD-NMR (STD) and reference-NMR (Ref) spectra of 2 mM complex-type carbohydrate in the presence of 20 μM Fab PG16; # denotes residual Tris; asterisk (in H6′G*) indicates overlapping signals with H5D and H5F. The STD enhancement for H6′G was estimated to be equivalent to its nonoverlapped geminal ^{1}H H6G.

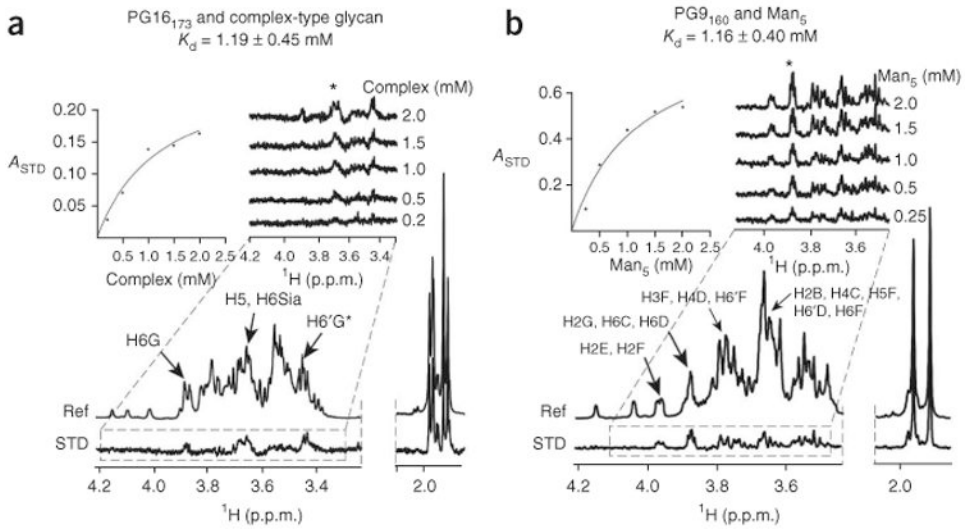

Figure 4.

PG16 binds complex-type glycans more tightly than $Man_5GlcNAc_2$, whereas PG9 prefers $Man_5GlcNAc_2$. (**a,b**) STD NMR analysis of glycan affinities. Complex type–glycan affinity for $PG16_{173}$, a PG16 mutant ($Asn100P_{HC}Arg$) that binds only glycan 173_{gp120} (**a**) and Man_5 affinity for $PG9_{160}$, a PG9 mutant ($Ser55_{HC}Arg$) that binds only glycan 160_{gp120} (**b**) are shown. (Fig. 8 shows wild-type affinities.) STD enhancements (0.5-s saturation time) as a function of carbohydrate concentration are shown as a series of stacked plots. K_d values were obtained from the initial slope of the best-fitted Langmuir binding curves (insets) for the STD amplification factor, A_{STD}, as a function of glycan concentration by keeping antibody concentration constant (20 μM). Asterisk denotes region integrated to obtain A_{STD} values by the equation $A_{STD} = (I_0 - I_{SAT})\ I_0 - 1\ ([L_t]/[P])$, where L_t and P are the total ligand and protein concentrations, respectively, and I_0 and I_{SAT} are the integrals of signals in the reference and difference spectra, respectively.

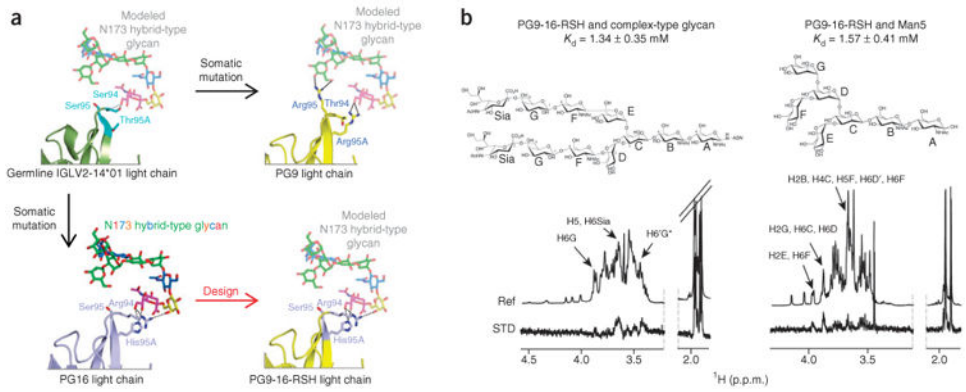

Figure 5.

Design and glycan recognition of PG9-16-RSH antibody. (**a**) Structure-based design. Ribbon representation of light chains interacting with hybrid-type N-glycan 173 are shown for initial germline recombinant of PG9-PG16 (IGLV2-14*01) (dark green and cyan, upper left), mature PG16 (light blue, lower left), mature PG9 (yellow, upper right) and PG9-16-RSH (yellow and light blue, lower right). Key light-chain residues at residues 94_{LC}, 95_{LC} and $95A_{LC}$ are labeled and colored cyan in the germline, yellow in the mature PG9 and light blue in the mature PG16, where they are arginine, serine and histidine (RSH), respectively. Saccharide subunits are colored as in Figure 1, and modeled glycan interactions are shown in semitransparent sticks. (**b**) Glycan recognition. STD-NMR (STD) and reference-NMR (Ref) spectra of 2 mM complex-type carbohydrate (right) and $Man_5GlcNAc_2$ (left) in the presence of 20 μM PG9-16-RSH antibody. K_d values (obtained as shown in Supplementary Fig. 3e from the initial slope of the best-fitted Langmuir binding curves for A_{STD} as a function of glycan concentration) are shown.

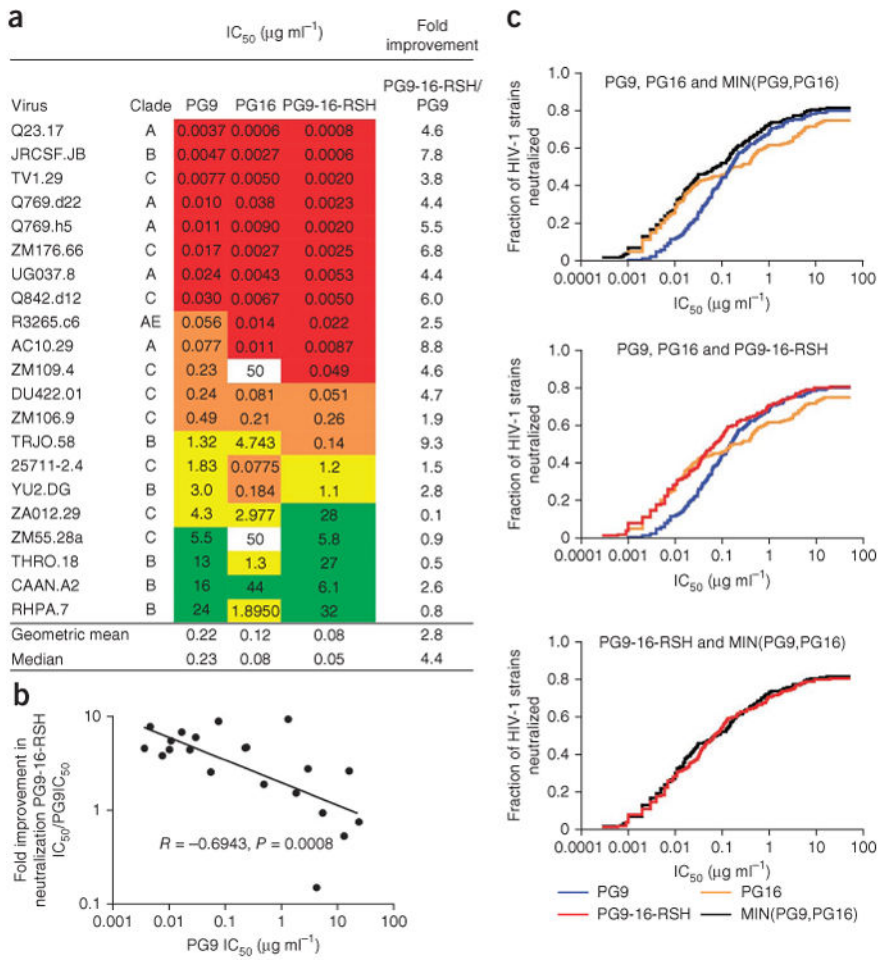

Figure 6.

Neutralization activity of PG9, PG16 and PG9-16-RSH. (a) Antibody neutralization is shown against a cross-clade panel of 21 pseudoviruses: red, $IC_{50} < 0.05$ μg ml^{-1}; orange, $0.05 < IC_{50} < 0.5$ μg ml^{-1}; yellow, $0.5 < IC_{50} < 5$ μg ml^{-1}; green, $5 < IC_{50} < 50$ μg ml^{-1}. The neutralization of PG9-16-RSH relative to PG9 is shown in the far-right column. (b) Correlation between PG9-16-RSH improvement as a function of PG9 potency. PG9-16-RSH is approximately five-fold more potent on viral isolates that are potently neutralized by PG9. Correlation on a 195-virus panel is shown in Supplementary Table 3. (c) Breadth/potency curve obtained from a panel of 195 HIV-1 strains. The fraction of HIV-1 strains neutralized (vertical axis) is shown graphed versus the neutralization potency of PG9, PG16, PG9-16-RSH and MIN(PG9-IC_{50},PG16-IC_{50}) (horizontal axis), where MIN(PG9-IC_{50},PG16-IC_{50}) refers to the lower IC_{50} of either PG9 or PG16 for each HIV-1 isolate.

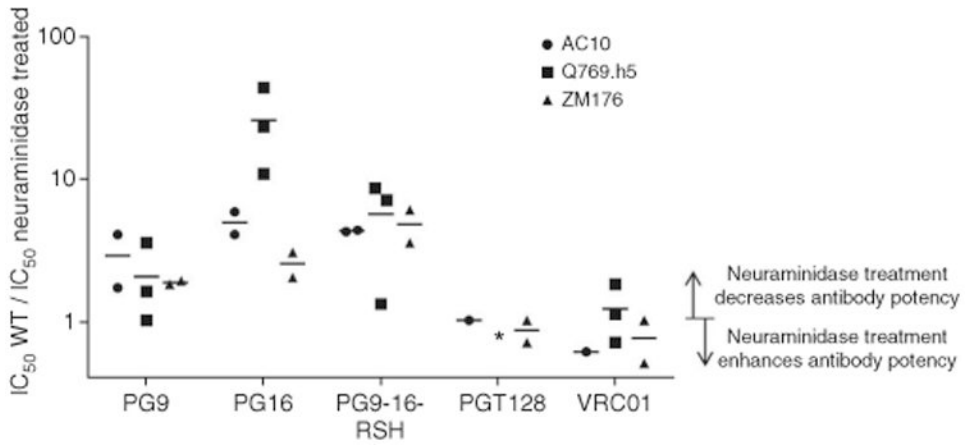

Figure 7.

Effect of sialic acid removal by neuraminidase treatment on PG9, PG16 and PG9-16-RSH antibody-mediated neutralization of HIV-1. Neuraminidase treatment and HIV-1 neutralization by PG9, PG16 and PG9-16-RSH are shown. Three pseudoviruses, AC10, Q769.h5 and ZM176, were either treated or not treated with neuraminidase, which removes sialic acid from complex-type glycans. Potency ratios of wild type (WT)/neuraminidase treated are shown for PG9, PG16, PG9-16-RSH, PGT128 and VRC01. Asterisk denotes inability of PGT128 to neutralize Q769.h5 strain.

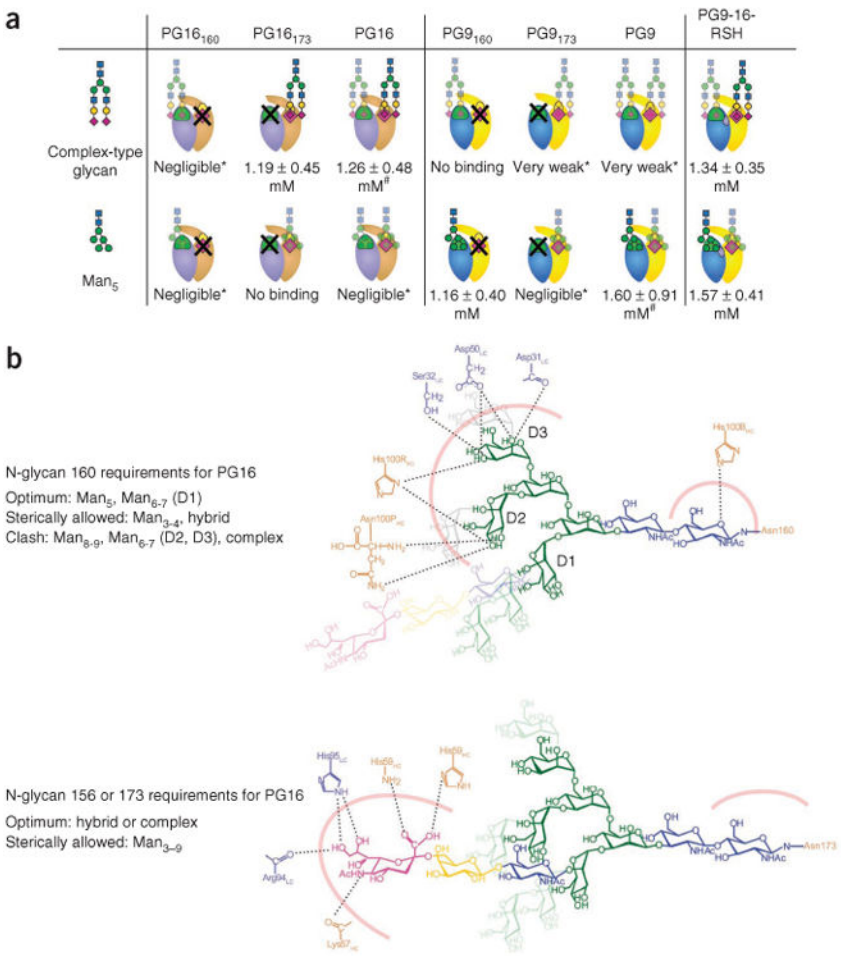

Figure 8.

Glycan recognition, binding affinities, and detailed interactions of PG16, PG9 and PG9-16-RSH. (**a**) Recognition and binding affinities for complex-type glycan and Man_5 binding to the individual glycan-binding sites of PG16, PG9 and PG9-16-RSH. Antibodies are depicted schematically with heavy and light chains in tan and light blue (PG16) and yellow and blue (PG9), respectively; antibody sites that bind glycan 160_{gp120} are green and those that bind glycan 156_{gp120} or 173_{gp120} are yellow and magenta, respectively. X denotes sites mutated to remove glycan binding. Glycan schematics are depicted in standard nomenclature and are semitransparent when recognition is poor. K_d values were obtained by fitting the data to a single-site binding model. ($^{\#}$ data did not fit a two-site model, consistent with very weak affinity for glycan at the second binding site; *very weak and negligible binding are described in Supplementary Fig. 3f.) (**b**) Detailed interactions governing binding of Man_5–Asn160 and complex-type glycan–Asn173 to PG16. Hydrogen bonds between heavy- and light-chain residues and sugar moieties of Man_5 (top) and hybrid-type glycan (bottom) are labeled, and the interfaces that also include hydrophobic interactions are represented by thick pink lines. Top, longer oligomannose branches whose interactions with PG16 are sterically allowed (D1 arm) are shown in pale green and those that would clash (D2, D3

arms) in pale gray. The $Asn173_{gp120}$ site (bottom) is optimal for binding hybrid or complex-type glycans (shown) but can also accommodate oligomannosides (transparent rings).

Table 1
Data collection and refinement statistics

	1FD6ZM109–PG16
Data collection	
Space group	$C222_1$
Cell dimensions	
a, *b*, *c* (Å)	81.1, 207.6, 87.6
Resolution (Å)	50–2.43 (2.52–2.43)[a]
R_{sym}	17.4 (48.6)
$I / \sigma I$	5.3 (1.35)
Completeness (%)	91.0 (61.4)
Redundancy	5.5 (3.2)
Refinement	
Resolution (Å)	45.1–2.44
Unique reflections	25,294
R_{work} / R_{free}	0.201 / 0.229
No. atoms	8,630
Protein	8,094
Ligand/ion	388
Water	148
B factors (Å^2)	
Protein	65.2
Ligand/ion	72.1
Water	43.9
r.m.s. deviations	
Bond lengths (Å)	0.002
Bond angles (°)	0.723

[a]Values in parentheses are for highest-resolution shell. The data set was collected from a single crystal.